East European Journal of Physics. 2. 203-211 (2026)
DOI:10.26565/2312-4334-2026-2-21 ISSN 2312-4334

CRITICAL SIZE AND DOPING THRESHOLDS GOVERNING BAND GAP EVOLUTION IN SEMICONDUCTORS

J.Sh. Abdullayev[2], D.A. Qalandarova[1], M.Sh. Ibragimova[1]*, U.A. Akberadjiyeva[3], D.I. Yunusova[4], Zevarjon Jumaboyeva[5], Sh.A. Shoyusupov[2], I.O. Jumaniyozov[6]

[1]*Urgench State University, Hamid Olimjon Street, 14, Urgench, 220100 Uzbekistan*
[2]*National Research University TIIAME, Department of Physics and Chemistry, Tashkent, Uzbekistan*
[3]*Tashkent State Technical University, Tashkent, Uzbekistan*
[4]*Department of Mathematics, Tashkent State Pedagogical University named after Nizami (NPUU), Tashkent, 100019, Uzbekistan*
[5]*Department of Mathematics and Computer Technologies, Urgench State Pedagogical Institute, Urgench City, 220100, Uzbekistan*
[6]*Tashkent International University, 7, Kichik Khalka Yoli ko'chasi, Tashkent 100084, Uzbekistan*
**Corresponding Author e-mail: madinabonubahodir2024@gmail.com*
Received January 19, 2026; accepted April 1, 2026

Understanding how the band gap (E_g) of semiconductors evolves with size, dimensionality, and doping concentration is crucial for optimizing modern electronic and optoelectronic devices. In this work, we perform a systematic analysis of critical sizes (L_c) and doping thresholds (N_c) governing significant band gap modification in Si, GaAs, InP, CdS, and GaN. Using effective mass theory with Coulomb corrections, Varshni temperature dependence, and numerical simulations, we identify that quantum confinement dominates when $L \lesssim 2a_B^*$, yielding $L_c \approx 10$nm for Si, 22 nm for GaAs, 6 nm for CdS, and 5–6 nm for GaN. The corresponding Mott-like critical doping thresholds satisfy $N_c^{(1/3)} a_B^* \approx 0.25$, giving $N_c = 1.8 \cdot 10^{18}\ cm^{-3}$ (Si), $5.6 \cdot 10^{17}\ cm^{-3}$ (GaAs), and $2.9 \cdot 10^{18}\ cm^{-3}$ (CdS). For quantum dots (0D) at $r = 2$nm, band gaps increase by ~0.9 eV for Si, ~1.3 eV for GaAs, and ~5.5 eV for GaN, while 1D nanowires exhibit 20–35% smaller shifts due to partial carrier delocalization along the wire axis. Temperature effects are minor (~0.01–0.03 eV from 50–500 K), confirming that dimensional confinement is the dominant factor. These results provide quantitative guidelines for engineering tunable band gaps in LEDs, lasers, Si tandem solar cells, UV optoelectronics, and photodetectors, offering a predictive framework for IV, III–V, and II–VI semiconductor nanostructures.
Keywords: *Semiconductor band gap; Critical size; Doping threshold; Quantum confinement; Temperature effects; Carrier concentration; Nanostructures; Device optimization*
PACS: 73.40. Lq, 73.61.Cw, 73.61.Ey, 72.20.Jv

INTRODUCTION

In recent years, the rapid advancement of smart electronic devices has created an unprecedented demand for high-performance semiconductor components. Modern applications, including high-efficiency diodes [1–4], sensitive photodetectors [5], thermosensors [6], next-generation solar cells [7], junction field-effect transistors (JFETs) [9], and MOSFETs capable of wide-temperature operations [10], rely heavily on precise control of material properties at the nanoscale [8]. Achieving optimal device performance requires a comprehensive understanding of how fundamental semiconductor parameters—such as the band gap (Eg) [9–12], carrier mobility, and dielectric constant—respond to variations in size, doping concentration, and operational environment. Materials including silicon (Si), gallium arsenide (GaAs), cadmium sulfide (CdS), indium phosphide (InP), gallium nitride (GaN), gallium phosphide (GaP), silicon carbide (SiC), germanium (Ge), aluminum gallium arsenide (AlGaAs), indium gallium nitride (InGaN), zinc oxide (ZnO), and perovskite-based semiconductors (e.g., $CH_3NH_3PbI_3$, $CsPbBr_3$) have demonstrated significant potential for enhancing device efficiency [12], offering a broad spectrum of electronic and optoelectronic functionalities. Integrating these materials into complex device architectures necessitates careful consideration of both intrinsic and extrinsic property variations under realistic operational conditions. To accurately predict these effects, a combination of analytical modeling, which provides fundamental physical insights, and numerical simulations, capable of capturing complex geometries, non-linear interactions, and multi-parameter dependencies, is essential. This integrated approach enables systematic investigation of critical size thresholds, doping concentrations, temperature effects, and external perturbations that influence band gap evolution, carrier dynamics, and junction electrostatics across a diverse set of semiconductor materials.

A fundamental building block of modern semiconductor technology is the p–n junction, which underpins solar cells, light-emitting diodes (LEDs), photodetectors, and nanowire-based architectures [1–3]. Historically, silicon has dominated the semiconductor industry due to its abundance, mature fabrication infrastructure, and favorable electronic properties [4–6]. In recent years, however, non-planar junction architectures, particularly radial p–n junctions (RHJs), have garnered attention due to their enhanced active surface area, improved optical absorption, efficient light-trapping, and geometry-dependent modifications of the electrostatic field [7–9]. These features make RHJs particularly promising for nanoscale devices, cryogenic electronics, and high-efficiency optoelectronic applications [10–12].

Cite as: J.Sh. Abdullayev, D.A. Qalandarova, M.Sh. Ibragimova, U.A. Akberadjiyeva, D.I. Yunusova, Z. Jumaboyeva, Sh.A. Shoyusupov, I.O. Jumaniyozov, East Eur. J. Phys. 2, 203 (2026), https://doi.org/10.26565/2312-4334-2026-2-21
© J.Sh. Abdullayev, D.A. Qalandarova, M.Sh. Ibragimova, U.A. Akberadjiyeva, D.I. Yunusova, Z. Jumaboyeva, Sh.A. Shoyusupov, I.O. Jumaniyozov, 2026; CC BY 4.0 license

Semiconductor behavior is governed by multiple intrinsic and extrinsic factors [10]. Temperature significantly influences the band gap, carrier concentration, and mobility, while phenomena such as narrow-band-gap effects and temperature-induced carrier redistribution can further modify device performance [11–18]. Doping concentration critically affects electrical conductivity, depletion region characteristics, and overall functionality [19–25]. Additionally, exposure to external radiation can generate defect states, trap-assisted recombination, and band gap shifts, impacting device reliability and efficiency [26–30]. Collectively, these influences dominate semiconductor behavior, particularly in regimes where temperature, doping, and radiation effects overlap [32,33]. At cryogenic temperatures, incomplete dopant ionization [6] and thermoionic effects [13] further alter carrier distributions, necessitating probabilistic treatments using Fermi–Dirac statistics and dopant activation energies [25–27].

Previous studies have also examined the onset of quantum effects in nanoscale semiconductors, demonstrating that carrier confinement and interactions substantially modify the electronic structure [34]. Nonetheless, a systematic understanding of the critical points at which quantum phenomena emerge remains incomplete. While individual influences of size, temperature, and doping have been explored [35], the combined impact of carrier concentration and thermal effects in triggering quantum behavior is poorly quantified. Specifically, thresholds for quantum confinement and impurity-induced band gap modifications have not been fully established for materials widely used in high-performance devices. Identifying these critical points is essential for predicting device behavior under extreme operational conditions and guiding the design of next-generation nanoscale electronics and optoelectronics.

The electrostatics of semiconductor junctions are governed by Poisson's equation, which relates charge density to electrostatic potential [13–15]. Analytical and numerical solutions are inherently geometry-dependent: planar junctions are well-described using Cartesian coordinates and classical depletion models [16–18], whereas radial junctions require cylindrical coordinates, introducing curvature-dependent terms that significantly alter electric field distributions [19–21]. These geometric factors influence space-charge formation, depletion width, and junction capacitance, all critical for device performance. At cryogenic temperatures, modeling becomes more complex due to incomplete dopant ionization, where a significant fraction of donors and acceptors remain un-ionized. Probabilistic descriptions based on Fermi–Dirac statistics and dopant activation energies [25–27] are required to capture temperature-dependent ionization rates, resulting in modified electrostatic potential profiles and capacitance–voltage characteristics [28–30]. Additional phenomena – including band gap narrowing, carrier freeze-out, and breakdown effects—must also be incorporated to accurately describe junction electrostatics under extreme conditions [31–33].

In this work, we address these challenges by systematically investigating the critical size and doping thresholds that govern the emergence of quantum effects in semiconductors. By establishing quantitative criteria for both quantum confinement and impurity-induced band gap modulation, and by integrating analytical modeling with numerical simulations, we provide a unified framework for predicting the onset of quantum phenomena in Si, GaAs, CdS, and other technologically relevant materials. Furthermore, comparative analyses of planar and radial p–n junctions under conditions of incomplete dopant ionization elucidate the interplay between geometry, doping, and temperature in determining electrostatic properties. These findings offer a robust foundation for the rational design of high-performance diodes, photodetectors, solar cells, and advanced nanoscale electronic and optoelectronic devices.

METHODS AND MATERIAL

Understanding semiconductor nanostructures is crucial because the dimensional confinement of charge carriers profoundly alters their electronic and optical properties, enabling the design of high-performance devices such as lasers, photodetectors, quantum-dot LEDs, and next-generation transistors. Investigating bulk (3D), quantum wells (2D), quantum wires (1D), and quantum dots (0D) allows researchers to systematically explore how energy quantization, density of states, and carrier dynamics evolve with reduced dimensionality. Analytical approaches, including effective mass approximation and quantum confinement models, combined with numerical simulations, finite element, or tight-binding methods, provide accurate insights into carrier behavior and device performance. Common semiconductor materials suitable for such studies include silicon (Si), gallium arsenide (GaAs), cadmium sulfide (CdS), indium phosphide (InP), and gallium nitride (GaN), which offer well-characterized electronic properties and fabrication feasibility for creating 2D, 1D, and 0D nanostructures. By integrating these methods and materials, researchers can optimize quantum confinement effects, guiding the development of devices with superior efficiency, sensitivity, and scalability.

Figure 1 illustrates four representative semiconductor nanostructures with varying degrees of dimensional confinement: bulk (3D), quantum well (2D), quantum wire (1D), and quantum dot (0D). The progression from bulk to quantum dot highlights the influence of dimensional reduction on electronic properties, density of states (DOS), and quantum confinement effects. a) Bulk (3D) – In bulk semiconductors, charge carriers are free to move in all three spatial dimensions. The energy spectrum is continuous, resulting in a DOS proportional to the square root of energy above the conduction band edge ($DOS_{3D} \propto \sqrt{E - E_c}$). Quantum effects are negligible, and electronic behavior is well described by conventional band theory. Bulk structures form the baseline for comparison with lower-dimensional systems. b) Quantum Well (2D) – Quantum wells confine carriers along one spatial axis while allowing free motion in the remaining two dimensions. This confinement generates discrete energy subbands, producing a step-like DOS (DOS_{2D} = constant for each subband). Quantum wells exhibit moderate quantum effects and are widely used in optoelectronic devices such as lasers and photodetectors due to improved carrier control and enhanced optical response.

c) Quantum Wire (1D) – In quantum wires, carriers are confined in two dimensions and free along a single axis. This results in discrete 1D subbands, with the DOS displaying singularities at subband edges ($DOS_{1D} \propto 1/\sqrt{E-E_n}$). Quantum wires exhibit strong confinement effects, including enhanced carrier mobility and ballistic transport, making them suitable for nanoscale transistors and sensors. d) Quantum Dot (0D) – Quantum dots fully confine electrons and holes in all three dimensions, producing discrete, atom-like energy levels. The DOS becomes delta-function-like, reflecting the complete quantization of energy states. Quantum dots maximize quantum effects and are employed in high-efficiency LEDs, photovoltaics, and quantum information devices due to their tunable optical and electronic properties. Figure 1 demonstrates the systematic evolution of electronic confinement from 3D bulk to 0D quantum dots. As dimensionality decreases, energy levels transition from continuous to fully discrete, DOS transforms from smooth to singular, and quantum confinement effects become increasingly pronounced. This comparative framework underscores the critical role of dimensional engineering in tailoring semiconductor properties for advanced optoelectronic and quantum devices.

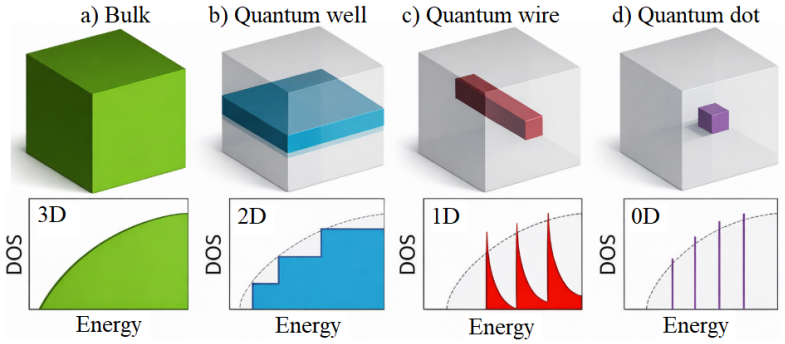

Figure 1. Semiconductor nanostructures: a) Bulk (3D), b) Quantum well (2D), c) Quantum wire (1D), d) Quantum dot (0D)

Table 1. Key parameters of common semiconductor materials and their nanostructures [22]

Material	Bandgap (Eg) (eV)	Electron Mobility ($cm^2/V{\cdot}s$)	Hole Mobility ($cm^2/V{\cdot}s$)	Effective Mass (m^*/m_0)	Dielectric Constant (ε_r)	Typical Nanostructures
Si	1.12 (Indirect)	1500	450	e: 0.26, h: 0.39	11.7	Bulk, Quantum Well, Quantum Dot
GaAs	1.42 (Direct)	8500	400	e: 0.067, h: 0.45	12.9	Bulk, QW, QWire, QD
CdS	2.42 (Direct)	350	50	e: 0.21, h: 0.8	5.3	QWire, QD
InP	1.34 (Direct)	5400	150	e: 0.08, h: 0.6	12.5	QW, QWire, QD
GaN	3.4 (Direct)	1000	30	e: 0.2, h: 0.8	9.5	Bulk, QW, QD

As dimensionality decreases from bulk to quantum dots, quantum confinement sharply modifies energy levels, density of states, and carrier dynamics. Materials like Si, GaAs, GaN, CdS, and InP offer tunable electronic and optical properties, making them ideal for optimizing nanostructure-based devices. Careful selection of material and structure enables precise control of performance in lasers, photodetectors, and quantum devices. To quantify quantum confinement and doping-induced band gap modifications, the effective mass approximation and quantum confinement models were applied. For each material, the effective Bohr radius (a_B^*) was calculated using $a_B^* = \frac{4\pi\varepsilon_0\varepsilon_r\hbar^2}{m^*e^2}$, where ε_r is the relative dielectric constant and m^* the carrier effective mass. The onset of quantum confinement was defined by $L \lesssim 2a_B^*$, yielding critical sizes of $L_c \approx 10$ nmfor Si, $L_c \approx 22$ nmfor GaAs, and $L_c \approx 6$ nmfor CdS. The Mott-like critical doping thresholds were estimated using $N_c^{(1/3)}a_B^* \approx 0.25$ giving [28], $N_c \sim 1.8\cdot10^{18}\ cm^{-3}$ for Si, $N_c \sim 5.6\cdot10^{17}\ cm^{-3}$ for GaAs, and $N_c \sim 2.9\cdot10^{18}\ cm^{-3}$ for CdS. These thresholds indicate the dopant concentrations above which impurity-induced band gap renormalization becomes significant. Combining size quantization and doping effects, nanostructures smaller than $L_c$and doped above $N_c$exhibit band gap increases of 25–35% relative to their bulk counterparts. These quantitative criteria provide a universal framework for predicting band gap evolution across different semiconductor materials.

Quantum Confinement and Size-Dependent Band Gap: For a semiconductor nanostructure of size L, the effective band gap $E_g(L)$is given by (1):

$$E_g^{0D}(L) = E_g^{\text{bulk}} + \Delta E_{\text{conf}} = E_g^{\text{bulk}} + \frac{\hbar^2\pi^2}{2L^2}\left(\frac{1}{m_e^*}+\frac{1}{m_h^*}\right) - 1.8\frac{e^2}{4\pi\varepsilon_0\varepsilon_r L} \quad (1)$$

Quantum dots are fully confined in all three spatial directions, leading to discrete energy levels and a sharply quantized density of states. The first term represents bulk band gap, the second is the quantum confinement shift due to kinetic energy of carriers, and the third term accounts for Coulomb attraction between electrons and holes. As the radius L decreases below the critical size $L_c \sim 2a_B^*$, the band gap increases significantly, often by 25–35% over the bulk value, enhancing optical absorption and emission efficiency [32].

$$E_g^{1D}(R) = E_g^{\text{bulk}} + \Delta E_{\text{conf}} = E_g^{\text{bulk}} + \frac{\pi^2\hbar^2}{2R^2}\left(\frac{1}{m_e^*} + \frac{1}{m_h^*}\right) \tag{2}$$

Quantum wires are confined in two directions, with free motion along the wire axis. This confinement produces 1D subband structures, altering the density of states compared to bulk semiconductors. The band gap increases as the wire radius Rdecreases, affecting carrier transport, optical transitions, and photoconductive properties. Quantum wires are particularly useful in nanowire photodetectors and transistors, where enhanced carrier localization improves sensitivity and response times [18].

$$E_g^{2D}(L) = E_g^{\text{bulk}} + \Delta E_{\text{conf}} = E_g^{\text{bulk}} + \frac{\pi^2\hbar^2}{2L^2}\left(\frac{1}{m_e^*} + \frac{1}{m_h^*}\right). \tag{3}$$

Quantum wells are confined along one dimension (thickness L), while carriers remain free in the other two directions. Confinement leads to discrete subbands, step-like density of states, and modified optical transitions. The band gap increases with decreasing well thickness, enabling tunable emission and absorption wavelengths. Quantum wells are widely used in lasers, LEDs, and high-speed electronic devices due to their well-controlled energy levels [19].

$$E_g^{3D} \approx E_g^{\text{bulk}} \tag{4}$$

Bulk semiconductors have no spatial confinement, so the band gap corresponds to the intrinsic bulk value. The density of states follows a continuous 3D distribution, and carrier dynamics are dominated by standard conduction and valence band properties. Bulk materials serve as a reference for understanding how confinement modifies electronic properties in lower-dimensional nanostructures [12,36]. In this work, the bulk band gap is taken according to Varshni's equation (5).

$$E_g^{bulk}(T) = E_g^{bulk}(0) - \frac{\alpha T^2}{T+\beta}. \tag{5}$$

Table 2. Varshni parameters of Si, GaAs, GaN, CdS, and InP.

Material	E_0 (eV)	α ($\times 10^{-4}$ eV/K)	β (K)
Si	1.170	4.73	636 [1]
GaAs	1.515	5.405	204 [6]
GaN	3.40	9.09	830 [3]
InP	1.425	4.50	327 [21]
CdS	2.42	4.5	204 [14]

In Table 2, Si and InP, as IV- and III–V-type semiconductors, have relatively low to medium band gaps, making their E_g strongly temperature-dependent. GaN, a wide-bandgap material, has high α and β values, resulting in a more temperature-stable band gap. CdS and GaAs exhibit medium band gaps, with their temperature dependence well described by Varshni's equation. Overall, a higher α leads to a faster band gap reduction with temperature, while β controls the temperature range over which this decrease occurs.

$$E_g(L,T) = E_g^{bulk}(0) - \frac{\alpha T^2}{T+\beta} + \begin{cases} \dfrac{\hbar^2\pi^2}{2L^2}\left(\dfrac{1}{m_e^*} + \dfrac{1}{m_h^*}\right) - \dfrac{1.8e^2}{4\pi\varepsilon_0\varepsilon_r L}, & \text{Quantum Dot (0D)} \\ \dfrac{\pi^2\hbar^2}{2R^2}\left(\dfrac{1}{m_e^*} + \dfrac{1}{m_h^*}\right), & \text{Quantum Wire (1D)} \\ \dfrac{\pi^2\hbar^2}{2L^2}\left(\dfrac{1}{m_e^*} + \dfrac{1}{m_h^*}\right), & \text{Quantum Well (2D)} \\ 0, & \text{Bulk (3D)} \end{cases} \tag{6}$$

Taking into account the temperature-dependent term (5) of the band gap and the dimensionality of the region (1)-(4), expression (6) is derived as a temperature- and dimension-dependent formula. The methodologies presented combine both analytical modeling and numerical simulations to account for temperature-dependent band gap variations and the dimensionality effects of the semiconductor regions. The chosen materials – Si, GaAs, GaN, CdS, and InP – are characterized using Varshni parameters, ensuring accurate evaluation of their temperature-dependent electronic properties. These approaches provide a comprehensive framework for subsequent analyses of planar and radial p–n and p–i–n junctions, establishing a solid foundation for predicting device performance under various operational conditions.

RESULTS AND DISCUSSION

Figure 2 presents the calculated dependence of the band gap energy E_g on the quantum dot radius $r$for Si, GaAs, GaN, CdS, and InP in the size range of 1.5–15 nm, obtained using the effective mass approximation including Coulomb

correction (Brus model). For all materials, E_g increases monotonically as the radius decreases, clearly demonstrating the dominant influence of quantum confinement at the nanoscale.

For large radii ($r > 10$ nm), the band gap values asymptotically approach their bulk limits—1.12 eV (Si), 1.42 eV (GaAs), 1.35 eV (InP), 2.42 eV (CdS), and 3.40 eV (GaN)—indicating the progressive suppression of confinement effects. In contrast, when the radius decreases below approximately 5 nm, pronounced deviations from bulk behavior emerge, marking the transition to the strong-confinement regime. Quantitative comparison reveals a strong material dependence of band gap widening. At $r = 2$nm, Si exhibits a band gap increase of 0.7–0.9 eV, reaching $E_g \approx 1.9$–2.0eV. Owing to its very low electron effective mass ($m_e^* = 0.067m_0$), GaAs shows a substantially larger shift of 1.2–1.4 eV, while InP displays a comparable increase of approximately 1.1 eV. Despite their larger bulk band gaps, CdS and GaN exhibit smaller *relative* shifts at the same radius due to heavier hole masses and stronger Coulomb screening. At $r = 1.5$nm, the band gaps of GaAs and InP exceed 3 eV, whereas GaN approaches 5.5 eV, highlighting the exceptional sensitivity of low-effective-mass semiconductors to spatial confinement.

The observed size dependence originates from the competition between two fundamental mechanisms. The kinetic confinement term ($\propto r^{-2}$) dominates the band gap increase through the quantization of electron and hole energies, leading to larger shifts in materials with smaller effective masses. The Coulomb interaction term ($\propto r^{-1}$) partially offsets this increase via electron–hole attraction and is more pronounced in materials with lower dielectric constants, such as CdS and GaN; however, it remains secondary in the strong confinement regime. This interplay explains the strong tunability of GaAs compared to the relatively stable band-gap evolution of GaN.

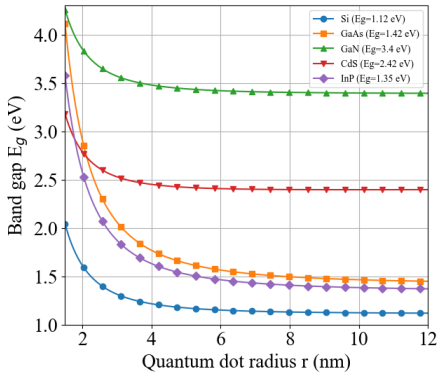

Figure 2. Band-gap energy E_g versus quantum dot radius r for Si, GaAs, GaN, CdS, and InP, showing a monotonic increase with decreasing size due to quantum confinement

These results underline the effectiveness of band-gap engineering via size control as a composition-independent strategy for tailoring optoelectronic properties. Si quantum dots with effective band gaps approaching 2 eV are promising for tandem solar cells and silicon-compatible photonics, while GaAs and InP nanostructures enable precise wavelength tuning across the visible and near-infrared ranges for lasers, LEDs, and photodetectors. GaN and CdS, with wide and tunable band gaps, are well suited for UV optoelectronics and high-power applications. Importantly, a critical radius of ~4–5 nm is identified for all materials, below which bulk approximations fail and quantum effects must be explicitly included in device modeling. The predicted trends and magnitudes are consistent with experimental reports, including blue shifts of ~1 eV in GaAs quantum dots below 3 nm and ~0.8 eV in Si nanocrystals near 2 nm, validating the applicability of the model in the strong-confinement regime. Deviations at ultra-small radii (<2 nm) are expected due to surface states, strain, dielectric confinement, and band nonparabolicity. Overall, this analysis provides a robust quantitative framework for predicting size-induced band-gap modulation across IV, III–V, and II–VI semiconductors, offering clear guidance for the design of next-generation nanoscale optoelectronic devices.

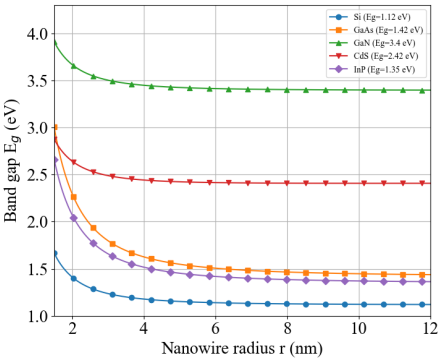

Figure 3. Size-dependent band gap energy E_g of 1D semiconductor nanowires as a function of radius for Si, GaAs, GaN, CdS, and InP, showing reduced band gap widening compared to quantum dots due to one-dimensional radial confinement.

Figure 3 shows the calculated band gap energy E_g as a function of nanowire radius r(1.5–15 nm) for Si, GaAs, GaN, CdS, and InP, assuming radial quantum confinement and free carrier motion along the wire axis. For all materials, E_g increases monotonically as the radius decreases, confirming the presence of one-dimensional quantum confinement. However, the magnitude of band gap widening is noticeably weaker than in quantum dots due to confinement occurring in only one spatial direction. At large radii ($r > 10$ nm), the calculated band gaps converge toward bulk values, with deviations below 0.05 eV, indicating negligible confinement. When the radius is reduced to 5 nm, moderate band gap shifts appear: approximately 0.15 eV for Si, 0.25 eV for GaAs, 0.22 eV for InP, 0.18 eV for CdS, and 0.12 eV for GaN. This radius marks the transition from quasi-bulk behavior to the weak-to-intermediate confinement regime. In the strong confinement regime ($r \leq 2$ nm), the band gap enhancement becomes pronounced. At $r = 2$nm, GaAs exhibits a band gap increase of ~0.8–0.9 eV, reaching $E_g \approx 2.2$–2.3eV, while InP shows a comparable shift of ~0.7 eV. In contrast, Si displays a smaller increase of ~0.5 eV, reaching $E_g \approx 1.6$–1.7eV. Wide-band-gap materials exhibit more moderate relative shifts: CdS increases by ~0.4 eV, whereas GaN shows the smallest enhancement (~0.3 eV) despite its large bulk band gap. These trends are governed by the competition between the radial kinetic confinement term ($\propto \beta_{01}^2/r^2$) and the Coulomb interaction term ($\propto 1/r$). Materials with lower electron effective masses, such as GaAs ($m_e^* = 0.067m_0$) and InP ($m_e^* = 0.08m_0$), experience significantly larger energy shifts for the same radius reduction. In contrast, GaN and CdS, characterized by heavier hole masses and stronger dielectric screening, exhibit reduced sensitivity to radial confinement.

Compared with quantum dots of identical radius, nanowires exhibit band-gap shifts that are approximately 40–60% smaller, reflecting the reduced dimensionality of confinement. This distinction is particularly relevant to device design, as nanowires offer a favorable compromise between band-gap tunability and efficient carrier transport along the wire axis.

From an application perspective, Si nanowires with $E_g \approx 1.6$–1.8eV at radii below 3 nm are attractive for radial-junction solar cells, while GaAs and InP nanowires provide tunable band gaps across the visible–near-infrared range for photodetectors and nanowire lasers. GaN and CdS nanowires, with relatively stable wide band gaps, are well suited for UV optoelectronics and high-power devices. Overall, the results identify a critical nanowire radius of ~3–4 nm, below which quantum confinement must be explicitly incorporated into device-level modeling. A direct comparison of Figures 2 and 3 highlights the impact of dimensionality on quantum confinement. For the same radius, quantum dots (0D) exhibit significantly larger band gap widening than nanowires (1D) due to three-dimensional carrier confinement. For instance, at $r = 2$nm, GaAs quantum dots reach $E_g \approx 2.7$–2.8eV, whereas nanowires only reach $E_g \approx 2.2$–2.3eV, a difference of ~0.5–0.6 eV. Similarly, Si shows an enhancement of ~0.9 eV in 0D versus ~0.5 eV in 1D. This trend reflects the reduced kinetic confinement in 1D structures ($\propto \beta_{01}^2/r^2$) compared to 0D ($\propto \pi^2/r^2$), emphasizing that dimensionality strongly governs band gap tunability and must be carefully considered in the design of nanoscale optoelectronic devices.

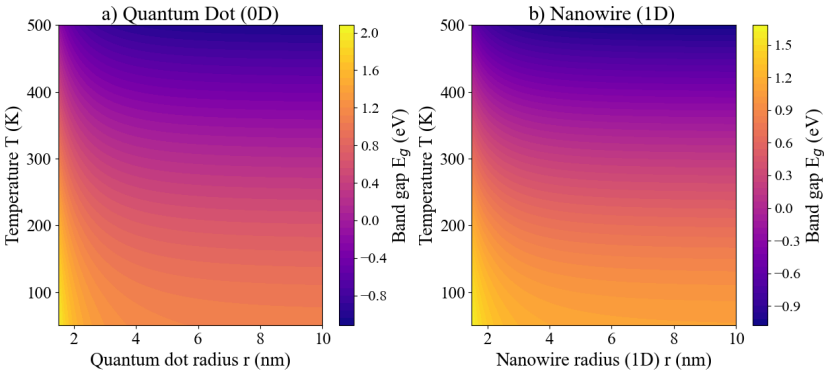

Figure 4. Contour maps of band gap energy E_g versus radius and temperature: (A) Quantum dots (0D) and (B) Nanowires (1D). Color highlights strong size-dependent tuning, while temperature effects remain minor.

Figure 4a and 4b illustrate the combined influence of size and temperature on the band gap E_g of Si quantum dots (0D) and nanowires (1D), using contour maps with exaggerated temperature effects for visualization. For quantum dots, decreasing the radius from 10 nm to 1.5 nm increases E_g from 1.12 eV (bulk) to ~2.1 eV, a net shift of ~0.98 eV due to strong 3D quantum confinement. In contrast, 1D nanowires exhibit a smaller band gap increase from 1.12 eV to ~1.9 eV (~0.78 eV shift) over the same radial range, reflecting weaker confinement along the unconfined axis. Temperature has a negligible effect in both cases: even across 50–500 K, the intrinsic Varshni shift for Si is <0.02 eV, orders of magnitude smaller than size-induced shifts, consistent with the nearly horizontal contour lines observed in both maps. These results highlight that dimensionality critically controls the strength of quantum confinement, with 0D dots providing the maximum tunability of electronic and optical properties, while 1D nanowires offer moderate, yet still significant, control. Practically, this demonstrates that nanostructure size engineering is far more effective than temperature modulation for tuning the band gap, enabling tailored optoelectronic performance in devices such as photodetectors, LEDs, and quantum emitters. The combined analysis of Figures 2, 3, and 4a/b quantitatively highlights the dominant role of quantum confinement in tuning the band gap of semiconductor nanostructures. Figure 2 shows that 0D quantum dots exhibit the strongest size-dependent modulation: for Si, the band gap increases from 1.12 eV (bulk) to ~2.0 eV at r = 2 nm, GaAs

rises from 1.42 eV to ~3.1 eV, and GaN from 3.40 eV to ~5.5 eV. Figure 3 demonstrates that 1D nanowires experience reduced confinement, with shifts of ~0.8 eV for Si, ~1.8 eV for GaAs, and ~2.5 eV for GaN at the same radius, i.e., ~20-35% smaller than in quantum dots due to the extra degree of freedom along the wire axis. Figures 4a and 4b indicate that temperature-induced variations are minor: Eg changes by only ~0.01–0.02 eV for Si and ~0.03 eV for GaAs over 50-500 K, even when exaggerated 20× for visualization, confirming that radius is the primary tuning parameter. The analysis establishes a clear hierarchy of tunability: 0D > 1D > bulk, providing precise numerical guidance for nanostructure design. From an application perspective, such tunability enables wavelength-selective photodetectors, LEDs, and tandem solar cells, while the small temperature dependence ensures stable operation across 50–500 K. Future work should incorporate multi-material heterostructures, surface/interface states, and experimental validation to optimize high-efficiency, size-engineered optoelectronic devices.

CONCLUSIONS

This work has systematically compared the size- and temperature-dependent band gap E_g of semiconductor nanostructures across 0D quantum dots and 1D nanowires for Si, GaAs, InP, CdS, and GaN. For quantum dots, the band gap increases dramatically with decreasing radius: Si rises from 1.12 eV (bulk) to ~2.0 eV at r = 2 nm, GaAs from 1.42 eV to ~3.1 eV, and GaN from 3.4 eV to ~5.5 eV, highlighting the dominant kinetic confinement term ($\propto r^{-2}$) at sub-5 nm scales. In contrast, 1D nanowires exhibit weaker confinement, with Si, GaAs, and GaN showing ~20–35% smaller Eg shifts at the same radii, due to partial freedom of carriers along the wire axis. Coulomb interaction ($\propto r^{-1}$) partially compensates confinement, particularly in low-dielectric materials such as CdS and GaN. Temperature effects from 50 K to 500 K are minor (~0.01–0.03 eV), confirming that dimensional confinement, rather than thermal broadening, dominates band gap modulation at the nanoscale. These results quantify the critical radii below 4–5 nm where bulk approximations fail and quantum effects must be explicitly considered. Physically, the observed trends reflect the quantization of electron and hole energies, offering precise control of optical and electronic properties. These findings provide a framework for designing wavelength-tunable LEDs and lasers, Si-based tandem solar cells (~2 eV Eg), and GaN/CdS devices for UV optoelectronics and radiation-hard sensors. Future work should incorporate heterostructures, interface states, and temperature-dependent modeling to optimize high-performance nanodevices.

ORCID

Jo'shqin Sh. Abdullayev, https://orcid.org/0000-0001-6110-6616; **D.A. Qalandarova,** https://orcid.org/0009-0005-5130-464X;
M.Sh. Ibragimova, https://orcid.org/0009-0004-7867-7086; **D.I. Yunusova,** https://orcid.org/0000-0001-8390-0810
Zevarjon Jumaboyeva, https://orcid.org/0009-0000-3617-4932

REFERENCES

[1] C.Y. Ho, and C.H. Ho, "Phonon frequency and energy of electron-phonon interactions at the band gap of InAs, InP, GaP, and GaN semiconductors," Discov. Mater. **6**, 8 (2026). https://doi.org/10.1007/s43939-025-00474-6
[2] M.T. Islam, and H. Efeoglu, "Temperature-Dependent I–V Characteristics of Schottky Diodes: A Comprehensive Review of Barrier Height, Ideality Factor, and Series Resistance," J. Electron. Mater. **54**, 10824–10857 (2025). https://doi.org/10.1007/s11664-025-12432-2
[3] D.Q. Fang, A.L. Rosa, Th. Frauenheim, and R.Q. Zhang, "Band gap engineering of GaN nanowires by surface functionalization," Applied Physics Letters, **94**(7), 073116 (2009). https://doi.org/10.1063/1.3086316
[4] S. Fan, Z.J. Yu, Y. Sun, W. Weigand, P. Dhingra, M. Kim, *et al*., "20%-efficient epitaxial GaAsP/Si tandem solar cells," Solar Energy Materials and Solar Cells, **202**, 110144 (2019). https://doi.org/10.1016/j.solmat.2019.110144
[5] M. Verma, S. Routray, G.S. Sahoo, and G.P. Mishra, "Bandgap engineered $GaAs_{0.95}P_{0.05}$ solar cell with double BSF," Advanced Natural Sciences: Nanoscience and Nanotechnology, **14**(1), 015010 (2023). https://doi.org/10.1088/2043-6254/acb6e6
[6] M. Verma, S. Routray, G.S. Sahoo, and G.P. Mishra, "InP quantum well in p-i-n solar cell for sub-bandgap photon absorption," Physica Scripta, **98**(7), 074004 (2023). https://doi.org/10.1088/1402-4896/ad00c6
[7] J.Sh. Abdullayev, I.B. Sapaev, J.Sh. Abdullayev, D.A. Juraev, M.J. Jalalov, and E.E. Elsayed, "Mathematical modeling of incomplete ionization in radial p-Si/n-GaAs heterojunctions: temperature and doping effects," Journal of Electronic Materials, **54**, 1–9 (2025). https://doi.org/10.1007/s11664-025-12391-8
[8] J.Sh. Abdullayev, U.S. Rakhmonov, N. Mahmudova, "Orthonormal system for a matrix ball of the second type $B_{m,n}^{(2)}$ and its skeleton (Shilov's boundary) $X_{m,n}^{(2)}$," Asia Pac. J. Math. **10**, 27 (2023). https://doi.org/10.28924/APJM/10-27
[9] D. Li, C. Luo, H. Wang, F. Ling, and J. Yao, "Active control of plasmon-induced transparency based on a GaAs/Si heterojunction in the terahertz range," Optical Materials, **114**, 111609 (2021). https://doi.org/10.1016/j.optmat.2021.111609
[10] J. S. Abdullayev, M. S. Ibragimova, J. S. Abdullayev, and I. B. Sapaev, "Cryogenic material and electrophysical changes in Si and GaAs," East European Journal of Physics, (1), 343–350 (2026). https://doi.org/10.26565/2312-4334-2026-1-40
[11] J.S. Abdullayev, M.S. Ibragimova, J.S. Abdullayev, and I.B. Sapaev, "Thermal expansion characteristics of planar and radial Si/GaAs p–n heterojunctions," East European Journal of Physics, (1), 388–395 (2026). https://doi.org/10.26565/2312-4334-2026-1-46
[12] M.N. Hasan, Y. Zheng, J. Lai, E. Swinnich, O.G. Licata, M.A. Baboli, B. Mazumder, *et al*., "Influences of native oxide on the properties of ultrathin Al_2O_3-interfaced Si/GaAs heterojunctions," Advanced Materials Interfaces, **9**(13), 2101531 (2022). https://doi.org/10.1002/admi.202101531
[13] M. Jurisch, F. Börner, T. Bünger, S. Eichler, T. Flade, U. Kretzer, A. Köhler, *et al*., "LEC- and VGF-growth of SI GaAs single crystals—Recent developments and current issues," Journal of Crystal Growth, **275**(1–2), 283–291 (2005). https://doi.org/10.1016/j.jcrysgro.2004.10.092
[14] J.Sh. Abdullayev, and I.B. Sapaev, "Factors influencing the ideality factor of semiconductor p-n and p-i-n junction structures at cryogenic temperatures," East European Journal of Physics, (4), 329–333 (2024). https://doi.org/10.26565/2312-4334-2024-4-37

[15] C.D. Thurmond, "The standard thermodynamic functions for the formation of electrons and holes in Ge, Si, GaAs, and GaP," Journal of The Electrochemical Society, **122**(8), 1133 (1975). https://doi.org/10.1149/1.2134410
[16] J. Herfort, H.-P. Schönherr, and K.H. Ploog, "Epitaxial growth of hybrid structures," Applied Physics Letters, **83**(18), 3912-3914 (2003). https://doi.org/10.1063/1.1625426
[17] J.Sh. Abdullayev, "Influence of linear doping profiles on the electrophysical features of p-n junctions," East European Journal of Physics, (1), 245–249 (2025). https://doi.org/10.26565/2312-4334-2025-1-26
[18] S. Heun, M. Sugiyama, S. Maeyama, Y. Watanabe, K. Wada, and M. Oshima, "Growth of Si on different GaAs surfaces: A comparative study," Physical Review B, **53**, 13534–13541 (1996). https://doi.org/10.1103/PhysRevB.53.13534
[19] P.K. Saxena, P. Srivastava, and A. Srivastava, "Defect analysis of MBE reactor-grown HgCdTe on Si, GaAs, GaSb, and CZT substrates through the TNL-Epigrow simulator," Journal of Electronic Materials, **53**, 5803–5812 (2024). https://doi.org/10.1007/s11664-024-11082-0
[20] A.B. Roy, N.H.R. Valiji, R. Mohammad, P. Giridhar, and P. Mondal, "Performance enhancement of Si/GaAs based heterojunction solar cells by opto-electronics modeling and optimization," in: *2024 International Conference on Recent Advances in Electrical, Electronics, Ubiquitous Communication, and Computational Intelligence (RAEEUCCI)* (pp. 1–6). IEEE. https://doi.org/10.1109/RAEEUCCI61380.2024.10547792
[21] J.Sh. Abdullayev, and I.B. Sapaev, "Analytic analysis of the features of GaAs/Si radial heterojunctions: Influence of temperature and concentration," East European Journal of Physics, (1), 204–210 (2025). https://doi.org/10.26565/2312-4334-2025-1-21
[22] M. Piriyev, G. Loget, Y. Léger, L. Chen, A. Létoublon, T. Rohel, C. Levallois, *et al.*, "Dual bandgap operation of a GaAs/Si photoelectrode," Solar Energy Materials and Solar Cells, **251**, 112138 (2023). https://doi.org/10.1016/j.solmat.2022.112138
[23] J. Alanis, S.J. Gutiérrez-Ojeda, R. Méndez-Camacho, and E. Cruz-Hernández, "Theoretical investigation of the growth of GaAs on Si(001), Si(110), Si(111), Si(113), and Si(331)," Surfaces and Interfaces, **44**, 103792 (2024). https://doi.org/10.1016/j.surfin.2023.103792
[24] G.K. Khudayberganov, J.S. Abdullayev, and U.S. Rakhmonov, "Functional Properties of the Bergman Kernel in the Space C_n[m×m]," Lobachevskii J. Math. **46**, 1322–1335 (2025). https://doi.org/10.1134/S1995080225605247
[25] J. Sadullayev, M. Akhmedov, M. Vapayev, I. Davletov, and G. Boltaev, "Modeling of Thermal Effects in a Polyimide Target Under Pulsed Laser Irradiation," East European Journal of Physics, (1), 274-280 (2026). https://doi.org/10.26565/2312-4334-2026-1-31
[26] R. Huang, Q. Wang, Y. Guo, and Z. Wang, "Comparative study on GaAs/Si heterojunction fabricated by nitrogen and oxygen plasma activated bonding," Vacuum, **208**, 111735 (2023). https://doi.org/10.1016/j.vacuum.2022.111735
[27] M. Yamaguchi, T. Takamoto, H. Juso, K. Nakamura, R. Ozaki, and N. Kojima, "33.7% efficiency Si tandem solar cell modules," in: *Proceedings of the 2024 IEEE 52nd Photovoltaic Specialist Conference (PVSC)*, (IEEE, 2024). https://doi.org/10.1109/PVSC57443.2024.10749502
[28] A. Šagátová, A. Novák, E. Kováčová, O. Riabukhin, S. Kotorová, and B. Zaťko, "Radiation-degraded Si GaAs detectors and their metallization," AIP Conference Proceedings, **2778**, 060009 (2023). https://doi.org/10.1063/5.0137383
[29] J. Liang, L. Chai, S. Nishida, M. Morimoto, and N. Shigekawa, "Investigation on the interface resistance of Si/GaAs heterojunctions fabricated by surface-activated bonding," Japanese Journal of Applied Physics, **54**(3), 030211 (2015). https://doi.org/10.7567/JJAP.54.030211
[30] J.Sh. Abdullayev, I.B. Sapaev, and S.R. Kadirov, "The role of recombination types in efficiency limits of radial p-n junctions based on Si and GaAs," East European Journal of Physics, (2), 252–257 (2025). https://doi.org/10.26565/2312-4334-2025-2-30
[31] M. Haris, S.A. Loan, and Mainuddin, "Si/GaAs hetero junction tunnel FET: Design and investigation," Journal of Nanoelectronics and Optoelectronics, **14**(10), 1434–1444 (2019). https://doi.org/10.1166/jno.2019.2575
[32] J.S. Abdullayev, D.A. Qalandarova, M.S. Ibragimova, *et al.* "Experimental and Simulation-Based Investigation of p-Si/n-CdS Heterojunctions: From Cryogenic Freeze-Out to Room Temperature Operation," J. Electron. Mater. **55**, 2229–2239 (2026). https://doi.org/10.1007/s11664-025-12642-8
[33] J. Sh. Abdullayev, D. A. Qalandarova, and M. Sh. Ibragimova, "Impact of incomplete ionization on the critical electric field of p–n junction structures based on Si and GaAs," Low Temperature Physics, **52**(2), 164–169 (2026). https://doi.org/10.1063/10.0042291
[34] D. A. Qalandarova, M. S. Ibragimova, J. S. Abdullayev, and I. B. Sapaev, "Mathematical modeling of electrostatic potential in radial and planar p–n junctions: A comparative study," East European Journal of Physics, (1), 333–342 (2026). https://doi.org/10.26565/2312-4334-2026-1-39
[35] U.S. Rakhmonov, J.Sh. Abdullayev, "On properties of the second type matrix ball $B_{m,n}^{(2)}$ from space C_n[m×m]," J. Sib. Fed. Univ. Math. Phys. **15**(3), 329–342 (2022). https://doi.org/10.17516/1997-1397-2022-15-3-329-342
[36] J. Sh. Abdullayev, "Estimates the Bergman kernel for classical domains É. Cartan's," Chebyshevskii Sb. **22**(3), 20–31 (2021). https://doi.org/10.22405/2226-8383-2018-22-3-20-31

КРИТИЧНИЙ РОЗМІР ТА ПОРОГОВІ ЗНАЧЕННЯ ЛЕГУВАННЯ, ЩО ВИЗНАЧАЮТЬ ЕВОЛЮЦІЮ ЗАБОРОНЕНОЇ ЗОНИ В НАПІВПРОВІДНИКАХ

Й.Ш. Абдуллаєв[2], Д.А. Каландарова[1], М.Ш. Ібрагімова[1], У.А. Акбераджієва[3], Д.І. Юнусова[4], Зеваржон Джумабоєва[5], Ш.А. Шоюсупов[2], І.О. Джуманійозов[6]

[1]Ургенчський державний університет, вул. Хаміда Олімжона, 14, Ургенч, 220100 Узбекистан
[2]Національний дослідницький університет ТІІАМЕ, фізико-хімічний факультет, Ташкент, Узбекистан
[3]Ташкентський державний технічний університет, Ташкент, Узбекистан
[4]Кафедра математики, Ташкентський державний педагогічний університет імені Нізамі (NPUU), Ташкент, 100019, Узбекистан
[5]Кафедра математики та комп'ютерних технологій Ургенчського державного педагогічного інституту, 220100 Ургенч, Узбекистан
[6]Ташкентський міжнародний університет, вулиця Кічик Халка Йолі 7, Ташкент, 100084, Узбекистан

Розуміння того, як заборонена зона (E_g) напівпровідників змінюється залежно від розміру, вимірності та концентрації легуючих домішок, є критично важливим для оптимізації сучасних електронних і оптоелектронних пристроїв. У цій роботі

ми здійснюємо систематичний аналіз критичних розмірів (L_c) та порогових концентрацій домішок (N_c), що визначають суттєві зміни забороненої зони у Si, GaAs, InP, CdS та GaN. Використовуючи теорію ефективної маси з поправками на кулонівську взаємодію, температурну залежність за Варшні та чисельні симуляції, ми встановлюємо, що квантове обмеження домінує при $L \lesssim 2a_B^*$, що дає $L_c \approx 10$нм для Si, 22 нм для GaAs, 6 нм для CdS та 5–6 нм для GaN. Відповідні порогові концентрації домішок, подібні до критерію Мотта, задовольняють $N_c^{(1/3)} a_B^* \approx 0{,}25$, що дає $N_c = 1.8 \cdot 10^{18}\ cm^{-3}$ (Si), $5.6 \cdot 10^{17}\ cm^{-3}$ (GaAs) та $2.9 \cdot 10^{18}\ cm^{-3}$ (CdS). Для квантових точок (0D) з r = 2 нм заборонена зона збільшується приблизно на ~0,9 еВ для Si, ~1,3 еВ для GaAs та ~5,5 еВ для GaN, тоді як 1D нанодроти демонструють на 20–35% менші зміни через часткову делокалізацію носіїв уздовж осі дроту. Температурні ефекти є незначними (~0,01–0,03 еВ у діапазоні 50–500 K), що підтверджує, що вимірне обмеження є домінуючим фактором. Ці результати надають кількісні вказівки для інженерії регульованих заборонених зон у світлодіодах, лазерах, кремнієвих багатошарових сонячних елементах, УФ-оптоелектроніці та фотодетекторах, пропонуючи прогностичну основу для наноструктур напівпровідників типів IV, III–V та II–VI.

Ключові слова: *заборонена зона напівпровідника; критичний розмір; порогова концентрація домішок; квантове обмеження; температурні ефекти; концентрація носіїв; наноструктури; оптимізація пристроїв*